Simulated structural and thermal properties of glassy and liquid germania

M. Micoulaut, Y. Guissani, and B. Guillot

Laboratoire de Physique Théorique de la Matière Condensée, CNRS UMR 7600,Université Pierre et Marie Curie, Boite 121, 4,
Place Jussieu, 75252 Paris Cedex 05, France

Structural, dynamical, and thermal properties of germanium dioxide are investigated with classical molecular dynamics simulations from the amorphous to the liquid state. Pair correlation functions and coordination numbers are computed under pressure change and show the progressive conversion of the tetrahedral network into an octahedral network, in agreement with experiments. The thermodynamical behavior of the liquid is investigated by means of an equation of state that allows a precise estimation of the compressibility. At low temperature, the diffusion constant D shows an Arrhenius law that progressively deviates when the temperature is increased. The overall comparison with simulated silica permits finally to outline not only the differences in the physical behavior of these two similar systems but also to stress the limitation of the employed germania potential.

PACS number(s): 61.20.Ja, 61.25.−f, 64.90.+b

I. INTRODUCTION

Germania (GeO$_2$) and silica (SiO$_2$) are archetypal simple glasses that form the basis for large families of noncrystalline materials. While silica has a considerable scientific and technological interest due to its abundance in geological systems and its use in domestic or window glasses, germania has received much less attention. Both have a tetrahedral local structure that serves as a corner-sharing building block to produce a three-dimensional network. However, differences with silicon dioxide emerge in the corresponding crystalline phases. Germanium dioxide can indeed exist in only two phases: a first α-quartz like phase with tetrahedrally coordinated germanium of low density $\rho=4.28$ g cm^{-3} and a local structure characterized by a bond distance $d_{\text{Ge-O}}=1.72$ Å and a second high-density phase with $\rho=6.25$ g cm^{-3} and a germanium-oxygen bond distance of 1.86 Å. The difference in density arises mostly from the local environment of the germanium atom, which is, respectively, fourfold (tetrahedral) and sixfold (octahedral) coordinated. Further polymorphic phase transformations are somewhat uncertain, such as the one induced by shock experiments at 600 kbar, leading to a so-called "*colombite-type*" GeO$_2$, or the synthesis of a FeN$_2$-type GeO$_2$ in the pressure range 250 to 350 kbar at temperatures over 1000 °C [1]. The structure of this high-pressure phase appears to be more dense [2] than rutile-like GeO$_2$.

Due to its homomorphism with silica, germanium dioxide is a useful system for the investigation of pressure- and temperature-induced changes in tetrahedral oxide glasses and melts. Indeed, the melting and glass transition temperatures of GeO$_2$ are much lower [3] ($T_m=1388$ K, $T_g=853$ K) as compared to silica [4] ($T_m=2003$ K, $T_g=1453$ K) and permits one to investigate the liquid over a large temperature range starting from the glass and far into the liquid phase up to 2500 K. The isomorphic nature of glassy GeO$_2$ and SiO$_2$ has been stressed from spectroscopic studies [5]. The structure of these tetrahedral systems has been studied in high-pressure experiments, first from permanently densified

samples [6] and recently with very accurate *in situ* experiments [7]. It turns out that octahedral germanium appears with increasing pressure. The pressure at which the conversion from fourfold to sixfold is almost complete is rather low, certainly lower than for the corresponding conversion in amorphous silica suggesting an increased structural sensitivity to pressure change for germania. Amorphous GeO$_2$ at ambient temperature shows indeed an abrupt change in bond length at around $P=7$ GPa [8], whereas smoother change occurs [9] in SiO$_2$ at higher pressure. The same kind of difference can be found [10] for the shift of the position of the first sharp diffraction peak (FSDP) with increasing pressure, as the signature of a reduction of medium-range order. Here, the sudden growth of the magnitude and width of the FSDP is observed for $P \simeq 5$ GPa in germania, while the corresponding behavior is found to be at about 13 GPa in the silica system. Richet *et al.* has measured [11] the corresponding energetics of pressure-induced densification. The sharp evolution in these different quantities with respect to pressure may lead to the suggestion that it is the signature of a first-order amorphous-amorphous transition [12]. Inspiration for this issue is provided by the very popular example of low and high-density amorphous water [13] that has attracted a lot of research on polymorphism both from the experimental [15] and the numerical side [14]. Tetrahedral disordered networks such as germanium [16], silicon [17], or silica [18] have been shown to have distinct amorphous phases, and since these results are obtained in a non-ergodic state, the nature and the question about the existence of the underlying transition(s) remain a challenging task. One may wonder whether or not this behavior is observable in GeO$_2$.

The interest in structural conversion of germanium dioxide has also attracted a lot of attention because of its anomalous behavior when an oxide network modifier is added into the structure. This phenomenon, known as the *germanate anomaly*, appears when 17% of Na$_2$O are added into the base germania network leading to a maximum in density, in glass transition temperature and in refractive index. This anomaly is not seen in the corresponding silicates, whereas it is almost independent of the nature of the modifier cation in ger-

manates. Structural studies, mostly by x-ray or neutron diffraction [19,20], Raman scattering [21], and extended x-ray absorption fine structure [22], have suggested that the increasing amount of octahedral germanium was responsible for the anomaly, an argument that apparently contradicts micro-Raman studies [23], which relate the growing presence of close-packed rings to the density increase. The study of the structural change of the basic network former GeO_2 with pressure can therefore give some clues for the understanding of the binary system. The structure and the vibrational density of states of amorphous GeO_2 has been inferred from Raman and infrared spectroscopy by Galeener and co-workers [24], while the germanium coordination number conversion has been specifically addressed from an *in situ* pressurized Raman analysis [25].

Surprisingly, no numerical simulations have been undertaken to study liquid and amorphous GeO_2 in detail up to recently [26], while extensive classical [27] and *ab initio* [28] molecular dynamics (MD) have been performed for silica. Woodcock and Angell performed the first MD simulation [29] of silica using effective interatomic potentials dealing with Coulombic interactions and Born-Mayer repulsions. The same kind of potentials have been used by various authors to determine the change in the structural properties and ring statistics under pressure in the amorphous state, the liquid, [30]. Germanium dioxide has been only studied in its crystalline form by several *ab initio* methods. Oeffner and Elliott [31] have fitted an empirical interatomic potential to an *ab initio* energy surface to account for the structure and the vibrational spectra of the α-quartz and rutile-like phases of GeO_2 and related issues have been investigated by means of an equation of state [32]. Several authors have used the same kind of approach (i.e., by fitting interatomic potential [33] or by performing density functional calculations [34]), to account for the pressure-induced structural change of the GeO_2 crystalline polymorphs [35].

We present here an MD study of vitreous and liquid germania that permits us to describe structural and thermodynamic properties of the system from the glassy state up to the critical point. The article is organized as follows. In Sec. II, we describe the methods of simulation used to study the liquid and glassy state of germania. In Sec. III, we discuss the glass transition and the structure of the simulated glass with respect to the experimental data. The evolution of the glass structure under pressure is also investigated. In Sec. IV is derived an analytical Birch-Murnhagan equation of state (BMEOS) for the liquid state by computing various (T, P, V) points. Finally, in Sec. VI summarizes our results and stresses the limitations of the employed potential.

II. METHODS AND CALCULATION

In the present calculation, we used the *ab initio* potential model developed by Oeffner and Elliott [31] to account for the description of vibrational spectra and lattice constants in GeO_2 polymorphs. The model employs a pairwise interatomic potential of the form

$$V_{ij}(r) = \frac{q_i q_j}{r} + A_{ij} e^{-B_{ij} r} - \frac{C_{ij}}{r^6} \quad (1)$$

which contains a Coulombic interaction, a Born-Mayer repulsion, and an attractive interaction. No three-body or

many-body interaction is included. In contrast with simulated silica where the divergence of the r^{-6} term produces some spurious behavior [36,37] at high temperature due to the unphysical attractive character at short distances, this does not happen in the present simulated germania. For the former, it is necessary to correct Eq. (1) by introducing additive [39] repulsive terms which fall off faster than $1/r^6$. In germania, the short-range repulsion term is one order of magnitude greater than the $1/r^6$ term thus making the overwhelming of the latter unlikely [31]. When performing MD calculations, the long-range Coulomb interactions have been evaluated by Ewald's method to ensure that the correct equilibrium thermodynamics and structure are obtained.

The present potential has been used to infer the local structure of crystalline GeO_2 and the cell parameters of the polymorphs. It is interesting to note that the Oeffner-Elliott potential has been able to reproduce the tetrahedral (α-quartz) to octahedral (rutile-like) conversion with pressure, together with a pressure-induced transition between the α and β quartz phase. The behavior with pressure appears therefore reliable, and one can expect that this should be the case in disordered systems as well. Furthermore, vibrational spectra show excellent agreement with experimental observation [31]. In this respect, we do expect that the same kind of local structural conversion with pressure can be properly simulated in the context of liquids and glasses and compared to experiment. However, some limitations of this model appear that we will discuss at the relevant places of interest.

We have simulated by MD in the (N, V, E) ensemble a sample of pure GeO_2 consisting of 512 oxygen and 256 germanium atoms. The equations of motion have been integrated using a leap-frog Verlet algorithm with a time-step of 1 fs. Starting from an initial temperature of 3000 K and cooling down to room temperature (300 K) to obtain the glass or heating up to study the high-temperature liquid. The liquid-vapor coexistence curve has been simulated using a different scheme that we describe below.

III. RESULTS AND DISCUSSION IN THE GLASS

A. Potential energy, enthalpy, and glass transition

The evolution of the liquid potential energy is represented in Fig. 1 for two different densities. One corresponds to the ordinary glass density $\rho_g = 3.66$ g cm^{-3} [38] and the other one at $\rho = 4.1$ g cm^{-3} to the pressurized liquid, both quenched at a cooling rate of 10^{12} K s^{-1}. Note that a factor $9RT/2$ is subtracted from the potential energy, which accounts for harmonic motions in the glassy state. The latter subtraction permits only to highlight the change in slope in the glass transition region as at low temperature, E_{pot}^0 is nearly constant (see also Fig. 2). The glass transition temperature deduced from the intersection of a linear high- and low-temperature extrapolation of the potential energy (inset of Fig. 1) is equal to $T_g \simeq 900$ K for $\rho = \rho_g$, a value that is much closer to the experimental value [4] (850 K) than in other related simulated systems. In silica, one finds, respectively, $T_g^{MD} \simeq 2000$ K with the Tsuneyuki potential [39] and $T_g^{MD} \simeq 2900$ K with the Van Beest (BKS) potential [40] to be
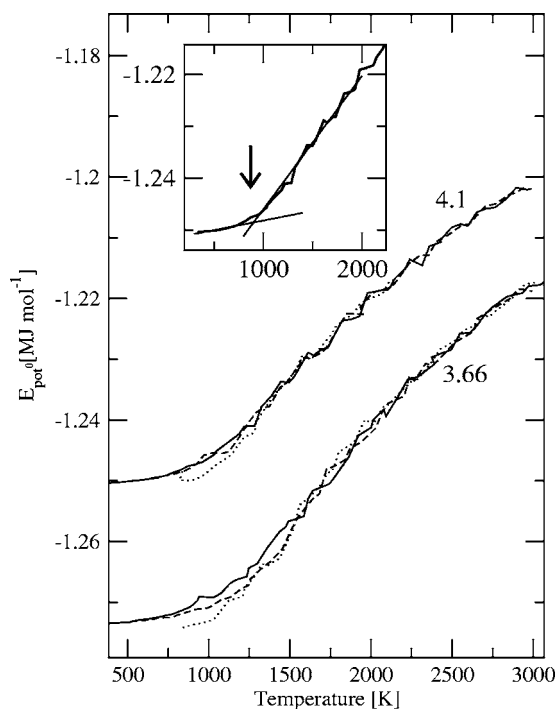
FIG. 1. Evolution of the liquid potential energy with temperature for two different densities $\rho_g = 3.66 \text{ g cm}^{-3}$ and $\rho = 4.10 \text{ g cm}^{-3}$. Both are represented after subtraction of $9RT/2$ to account for the harmonic motions in the glassy state upon cooling (solid line) and heating (broken line). The dotted curves correspond to a heating after relaxation of the glass during 1 ns at 800 K. For clarity, the upper curves have been shifted upwards by 25 kJ mol^{-1}. The inset shows the high- and low-temperature linear extrapolation that serve to roughly estimate T_g (here $\rho = 4.1 \text{ g/cm}^3$)

compared to $T_g^{exp} = 1450$ K, while in GeSe$_2$, it is respectively found $T_g^{MD} = 1000$ K and $T_g^{exp} = 750$ K [41]. These discrepancies between simulated and experimental T_g's are usually attributed to the unrealistic quenching rates that are applied, but we mention that fair agreement between simulation and experiment can be found in other systems as illustrated by the recent example of vitreous selenium [42]. We discuss this issue below.

Upon reheating the system from ambient temperature, no clear signature of enthalpic overshoot appears for $\rho = 4.1 \text{ g cm}^{-3}$, but a significant lowering of the potential energy is found when the system is relaxed at 800 K $\simeq 0.9 T_g^{MD}$. For an aging time of 1 ns at this temperature close to T_g, the system is able to explore the potential energy landscape to lower its potential energy. We furthermore notice that the lowering of the potential energy is more pronounced in the system at ρ_g as compared to the system at $\rho = 4.1 \text{ g cm}^{-3}$. The latter has an increased number of six-coordinated germanium atoms (see below), which produces a global increase of the stiffening of the structure [43,44] leading to less available internal degrees of freedom during landscape sampling at $T \simeq 0.9 T_g^{MD}$. The increase of density from ρ_g to $\rho = 4.1 \text{ g cm}^{-3}$ produces a slight variation in the potential energy profile.

Using a different numerical scheme allowing usually to follow the liquid-vapor coexistence curve [45], we obtain
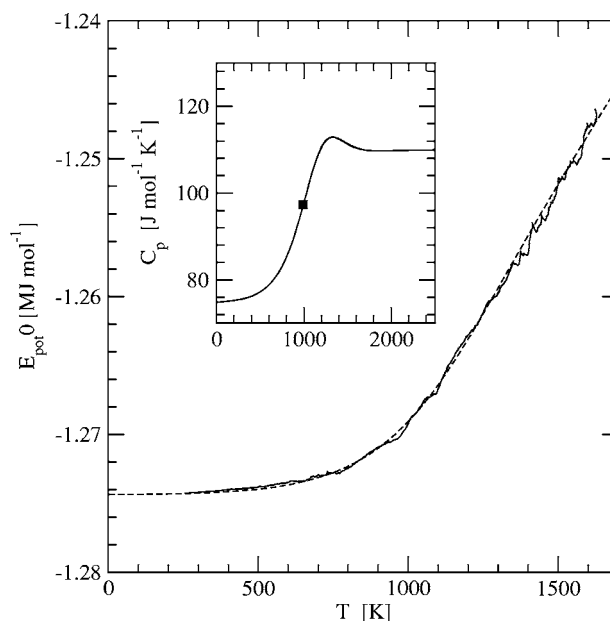

FIG. 2. Liquid potential energy (solid line) with temperature from a different cooling scheme (see below) together with a fit (broken line) that permits to extract the heat capacity (inset). The filled box corresponds to the inflexion point of C_p.

almost the same trend and values for the potential energy with respect to temperature (Fig. 2) when cooling the liquid along this line. Notice that in this case, the density of the simulated glass formed upon cooling is found to be around 3.7 g cm^{-3} and pressure is zero, again in close agreement with experiment. The enthalpy of the simulated system $H = E + PV$, that is represented in Fig. 3, shows a reasonable agreement with enthalpy data of liquid and glassy GeO$_2$ obtained from drop calorimetric measurements [46]. The computation of H takes into account a low temperature quantum correction (6.52 kJ mol^{-1}) of the specific heat of the glass [46] evaluated from the excess specific heat between the linear extrapolation of the liquid and the low-temperature glass. An analytical fit permits to extract the heat capacity from the computed potential energy (inset of Fig. 2) and the inflexion point of the latter quantity yields a glass transition temperature at 990 K.

We evaluate the specific heat jump ΔC_p at the glass transition to be of about $\Delta C_p = 38 \text{ J K}^{-1} \text{ mol}^{-1}$. Angell and
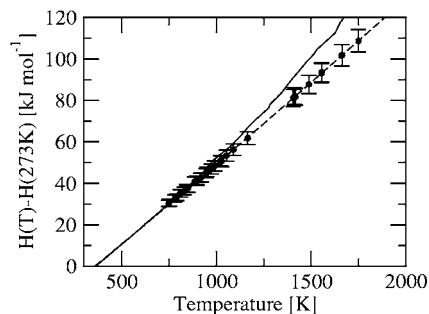

FIG. 3. Computed enthalpy of the liquid and glass phase $H(T) - H(273)$ (solid line) compared to calorimetric data from Richet [46] and a polynomial expansion (broken line) of $H(T)$ from Richet and Bottinga [47].
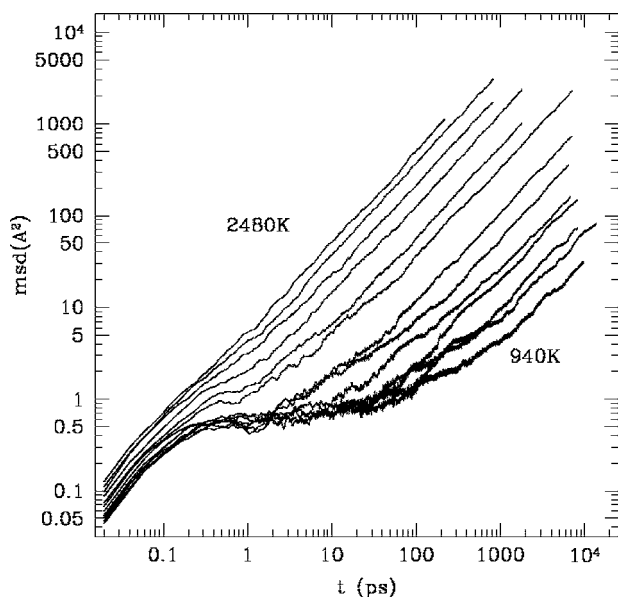
FIG. 4. Time dependence of the mean-squared displacement of oxygen for different temperatures ranging from 2500 to 920 K.
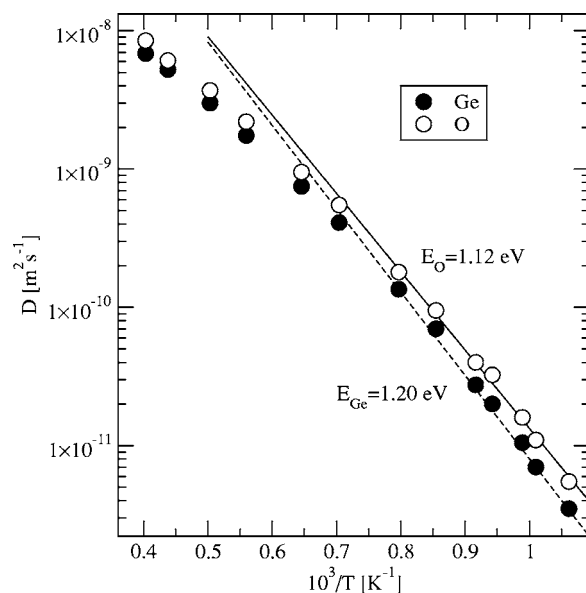

FIG. 5. Arrhenius plot of the germanium and oxygen diffusion constants. Solid and broken lines: Arrhenius fits to the data at low temperatures with the displayed activation energies.

Tucker [48] measured a value of 7.4 J mol^{-1} K^{-1} by differential scanning calorimetry with a fast heating rate of 40 K min^{-1}. Richet [46] estimated ΔC_p to be of the order of several percent of C_p in the glassy state, which was 75 J mol^{-1} K^{-1}. All these values are somewhat lower than our computed one. Recently, a technique using a modulated temperature [49] signal has permitted to extract ΔC_p that is almost unpolluted from kinetic events and the measured $\Delta C_p = 3.66$ J mol^{-1} K^{-1}, which is much lower [50] than previously reported values.

B. Dynamics

In order to estimate the level of accuracy reached by the Oeffner-Elliott potential to describe the liquid-glass transition in germania, we have computed the mean-square displacement of a tagged atom of type α in the melt; namely,

$$\langle r^2(t) \rangle = \frac{1}{N_\alpha} \sum_{i=1}^{N_\alpha} \langle |r_i(t) - r_i(0)|^2 \rangle, \qquad (2)$$

where N_α is the number of atoms α. The time dependence of this quantity for the oxygen atom is shown in Fig. 4 for various temperatures between the low viscosity liquid at $\simeq 2500$ K and the glass transition temperature evaluated in the present simulation ($\simeq 900$ K). The diffusion constant D can be obtained via the Einstein relation limit $D = \lim_{t \to \infty} \langle r^2(t) \rangle / 6t$. Both D_{Ge} and D_O are plotted in Fig. 5. As expected for a strong glass former, the temperature behavior is Arrhenius-like $[D \propto \exp(-E_A / k_B T)]$ when approaching T_g, a trend also observed in simulated silica [51]. From the experimental point of view, we are aware of only one published data [52] at only one temperature ($T = 1440$ K) for which the oxygen diffusion constant amounts to $D_O = 7 \times 10^{-14}$ m^2 s^{-1}, a value considerably lower than the simulated value at the same temperature

(5.8×10^{-10} m^2 s^{-1}). This discrepancy appears to be surprising at a first glance since the T_g is slightly higher than the experimental one (900 K instead of 850 K), as mentioned earlier.

In fact, this finding reveals a more serious problem when it concerns simulating strong glass formers like silica and germania. For the two melts, the evaluation of the viscosity with temperature is well documented [53] from the high-temperature liquid to the low-temperature glass. From the Eyring relation

$$\frac{k_B T}{\eta D} = \lambda = \text{const}, \qquad (3)$$

one is able to deduce an average diffusion coefficient knowing the viscosity η and postulating a reasonable value for λ the diffusion length (an hopping length in the Eyring theory [54]). In silicate melts (e.g., Na$_2$SiO$_3$), the Eq. (3) relation holds very well [55] with $\lambda \simeq 2.8$ Å, a distance typical of Si-Si and O-O separation in these melts. Assuming that this value of 2.8 Å holds for germania and silica as well, we have displayed in Fig. 6 the "*experimental*" diffusion constant for these two systems as a function of T_g / T, where the T_g are their known glass transition temperatures. Also displayed are our simulation results of D for germania and that for simulated silica by Kob *et al.* [51]. In the latter cases, T^{MD} is equal to 900 K for germania and 2850 K for silica [40]. Although the simulated curves exhibit the same trend than the experimental ones, namely, the silica and germania curves intersect each other at around $T_g / T \simeq 0.9$ (silica being less viscous at low temperature than germania and vice versa at high temperature), the simulated curves are shifted towards higher diffusivity by several orders of magnitude. To check the validity of our approach, we have reported the experimental values of D_O for silica and germania given in the
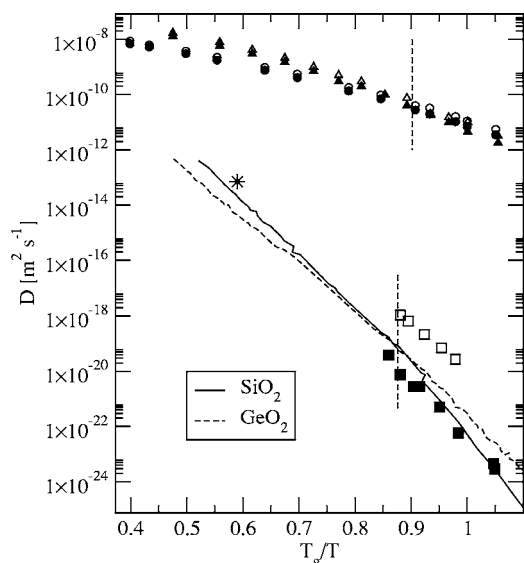
FIG. 6. Diffusion constants of germania (same symbols as Fig. 5) and silica (Si filled triangles, O open triangles, [51]) compared with "Eyring" diffusion constants [Eq. (3) using $\lambda = 2.8$ Å and the experimental viscosities for SiO_2 and GeO_2]. Also shown are the experimental measurements of the silicon (filled boxes) and oxygen (open boxes) diffusion in silica [56,57] and the oxygen diffusion in germania ($*$, Ref. [52]). The vertical broken line points out the approximate diffusivity cross-over at $T_g/T = 0.9$ between silica and germania (see text for details).

literature and we see that they closely match with the Eyring prediction using $\lambda = 2.8$ Å. Thus, the immediate implication of Fig. 6 is that the simulated melts are both too fluid with respect to the real ones. In other words the simulated systems are too much fragile and consequently their glass transition temperature should be found in a temperature range much lower than that found experimentally. Thus, we speculate that by using an appropriate cooling rate and a system size much larger (by several orders of magnitude) than used up to now, the apparent liquid-glass transition should appear at temperatures much lower than 850 K for our simulated germania and 1450 K for silica simulated with the BKS potential (see, however, [58]). Work in this direction is currently under consideration. Finally, a qualitative explanation for this behavior is that in strong glass formers like germania and silica (as compared with fragile liquids like water [13]), the free energy barriers become very high with respect to $k_B T$ when approaching T_g. Hence, the viscosity of the supercooled liquid is several orders of magnitude greater in a strong liquid than in a fragile liquid (e.g., at $T_g/T \simeq 0.5$, $\eta = 10^{-2}$ Pa s in liquid water [13] and 10^3 Pa s in silica or germania [53]). Thus, in a simulation using a small system size (a few hundred of molecules), the population of particles for a given temperature able to bypass the free energy barrier growing up when approaching T_g becomes virtually zero as soon as the energies are higher than a few $k_B T$. Upon cooling, the system leaves the liquid regime precociously to enter the glassy phase and is only weakly affected by the applied cooling rate. In fact, with system sizes generally investigated by simulation, the liquid-glass transition occurs as soon as the diffusion coefficient is about 10^{-12} m^2 s^{-1}, i.e., when the
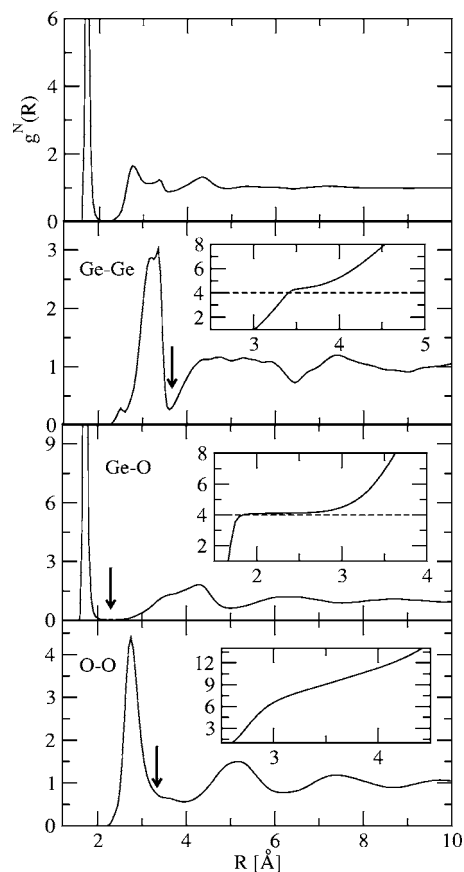

FIG. 7. Pair distribution functions $g_{ij}(r)$ for amorphous germania, together with the total neutron distribution function $g^N(r)$. The arrows indicate the approximate position $r = r'$ of the minimum and the inserts represent the corresponding running coordination numbers for the partials.

viscosity lies in the range about $1 - 10$ Pa s. Thus, to investigate liquids exhibiting much higher viscosities (in the $10^2 - 10^4$ Pa s range), it will require much higher system sizes, certainly several orders of magnitude larger than the present simulations.

C. Structure of the glass

Atomic trajectories from the MD simulations have been used to compute positional correlations in the vitreous state. The partial pair distribution functions $g_{ij}(r)$ are shown in Fig. 7 and determine the short-range order in the glass, out of which can be extracted the bond distances. A striking feature of the computed distribution functions is the sharp peak in g_{GeO} at $r = 1.72$ Å, which is clearly separated by a gap from all further variations with respect to r, leading to an oxygen well-defined environment for each germanium atom, typical of a network glass. Additional evidence of this feature is provided by the running coordination numbers of the different (i, j) pairs, which are the integrals over r of the partial distribution functions (insets of Fig. 7). As one can see, at the first minimum $r = r'$ of g_{GeGe}, it is found $n_{GeGe}(r') = 4.4$, thus meaning that each germanium atom is surrounded by somewhat more than four germanium atoms. This provides evi-

TABLE I. Simulated bond distances r_{ij}, bond angles of vitreous germania at 300 K, compared to experimental findings.

i-j	r_{ij}(Å)
Ge-Ge	Calc: 3.32
	Obs [61]: 3.16±0.03
Ge-O	Calc: 1.72
	Obs [61]: 1.73±0.03
O-O	Calc: 2.81
	Obs [61]: 2.83±0.05
i-j-i	
Ge-O-Ge	Calc: 159°
	Obs [62]: 130°
O-Ge-O	Calc: 108°
	Obs [62]: 109°

FIG. 8. Simulated total neutron $T(r)$ (solid line) of vitreous germania, compared with results from neutron diffraction (points [63]).

dence for the quasitetrahedral character of the network. At the corresponding r' of g_{GeO} and g_{OO}, it is, respectively, found that $n_{GeO}=4.1$ and $n_{OO}=8.2$. The coordination numbers obtained clearly indicate that the network is made mostly of GeO$_{4/2}$ tetrahedra connected by corners and that a linking oxygen has eight oxygen neighbors, six of them being part of the two connected tetrahedra. These observations are in agreement with the general accepted structural picture of glassy GeO$_2$, for which no edge-sharing GeO$_{4/2}$ tetrahedra are observed [61].

Tables I and II summarize the short-range structural results (bond distances, bond angles, coordination numbers) obtained from the simulation, together with experimental findings deduced from a combination of x-ray and neutron data [61,62]. Here, one can see that the agreement is fair, except for the Ge-Ge bond distance, which has been slightly overestimated. This feature may arise from the fact that the present interatomic potential does not contain any germanium-germanium interaction except the Coulombic long-range term, in contrast with the Matsui potential [33]. We notice also that except for the Ge-Ge distance, the bond distances are recovered at the correct density ρ_g of the glass, a situation that contrasts with the MD simulation of silica using the same kind of interatomic pairwise potential [39]. For the latter, there is need to increase the density up to $\rho=2.5$ g cm^{-3} (while the experimental ρ_g is 2.2 g cm^{-3}) in order to obtain [39] the correct bond distances and pressure ($P \simeq 0$). In germania, one major consequence of the small overestimate in germanium-germanium bond distance is that the intertetrahedral bond angle Ge-O-Ge becomes also

TABLE II. Computed coordination numbers at the distance cutoffs r' correspondings to the minimum in the partial distribution functions.

i-j	n_{ij}	r'[Å]
Ge-Ge	4.4	3.60
Ge-O	4.1	2.30
O-O	8.2	3.30
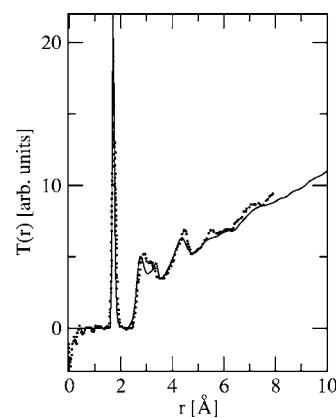
greater than its measured value from NMR spectroscopy [62], whereas the O-Ge-O is in agreement with the results from neutron and x-ray scattering data [61,63]. However, the total neutron pair correlation function $T(r)$ obtained from the pair correlation functions is in good agreement with the experimental results (Fig. 8) from Hannon and co-workers [63]. The $T(r)$ function has been calculated from

$$T(r) = 4\pi r \rho_g g^N(r), \qquad (4)$$

where $g^N(R)$ is the neutron distribution function (see Fig. 7) obtained from the Fourier transform of the scattering factor (see below) and has been defined by

$$g^N(r) = \frac{\sum_{i,j} c_i b_i c_j b_j g_{ij}(r)}{\left[\sum_i b_i c_i\right]^2}, \qquad (5)$$

where the coherent neutron scattering length b_i of germanium and oxygen has been used [64] ($b_{Ge}=8.193$ fm and $b_O=5.805$ fm) and c_i is the concentration of atom i. As one can see, the global trend of $T(r)$ is recovered which validates the present simulation in the glass, and can serve as a basis for the MD structural characterization of diffraction measurements from Hannon and co-workers [63]. The peak at 1.72 Å is obtained, but also the twin peak distribution seen around 3 Å emerges from the oxygen-oxygen and germanium-germanium bond correlations, although the latter produces a shouldered instead of a well-resolved peak in experiment. The secondary peak observable at 4.5 Å arises from the secondary Ge-O correlation (see also Fig. 7). Note also that the peak at 5.5 Å is not obtained due to the absence of any clear peak in the Ge-Ge pair distribution function (Fig. 7) in this range.

D. Static structure factors

Structural correlations in glassy GeO$_2$ can be extracted from the partial scattering functions, according to
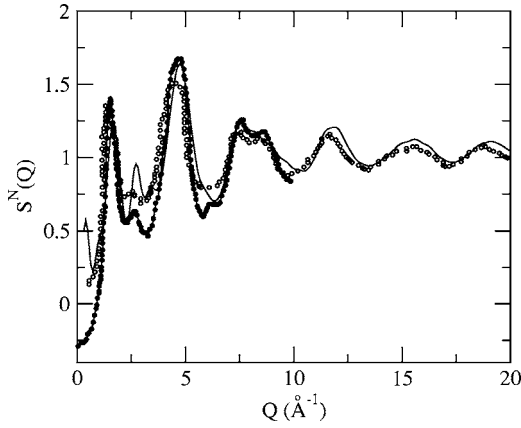
FIG. 9. Simulated neutron structure factor $S^N(Q)$ (solid line) of vitreous germania, compared with results from neutron diffraction from Price *et al.* (open circles [61]) and Hannon *et al.* (filled circles [63]).

$$S_{ij}(Q) - \delta_{ij} = 4\pi\rho\sqrt{c_ic_j}\int_0^\infty r^2[g_{ij}(r)-1]\frac{\sin(Qr)}{Qr}dr, \quad (6)$$

which lead to the neutron structure factor.

$$S^N(Q) = \frac{\sum_{i,j} b_ib_j\sqrt{c_ic_j}[S_{ij}(Q)-\delta_{ij}+\sqrt{c_ic_j}]}{\left[\sum_i b_ic_i\right]^2}. \quad (7)$$

For vitreous germania, the MD results for the neutron static structure factor $S^N(Q)$ are shown in Fig. 9, together with recent experimental results from Hannon *et al.* [63] and Price *et al.* [65]. There is fair agreement between the MD simulation and the experiments. The position of the first sharp diffraction peak (FSDP) at around 1.5 Å^{-1} is recovered, whereas the simulated peak at $Q \simeq 2.5$ Å^{-1} (corresponding to a correlation length of $L=2\pi/Q=2.51$ Å) is slightly too intense as compared with the experimental results which display only a shallow peak at that position. One should note that this peak is more clearly seen in x-ray scattering results [65] and that the FSDP at 1.5 Å^{-1} and the peak at 2.5 Å^{-1} have been found from partial structure factors by Waseda *et al.* [66]. Additional information arises from the computed partial structure factors $S_{ij}(Q)$, which permit to infer the origin of the peaks appearing in the total scattering function $S^N(Q)$ of Fig. 9. It appears from Fig. 10 that the FSDP mostly shows up in the S_{Ge-Ge} and S_{Ge-O} partials, meaning that cation correlations dominate the intermediate range order in vitreous germania, a situation that is also found in various other oxide or chalcogenide glasses [28,67,68]. Other features can be evidenced such as the peaks at $\simeq 4.5$ Å^{-1} again in the S_{Ge-Ge} and S_{Ge-O} partials that are usually associated with topological short-range order [69]. On the other hand, one can see that the too intense simulated peak found around 2.5 Å^{-1} arises from the $S_{Ge-Ge}(Q)$ function that is usually more intense in the x-ray scattering factor [70]. In fact, recent combined neutron and x-ray measurements highlight the role played by the respective weighting factors [71] to account
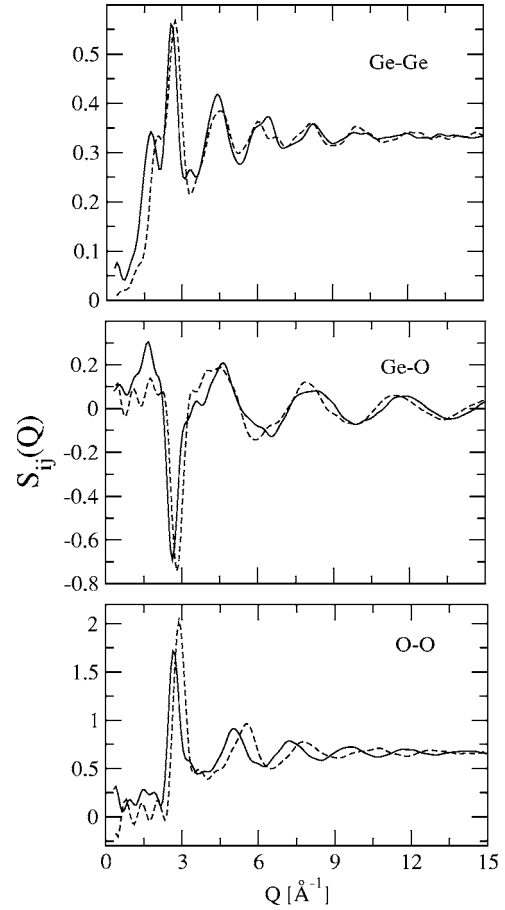

FIG. 10. Partial static structure factors $S_{ij}(Q)$ for vitreous germania at 300 K (solid lines). Same partials for a GeO$_2$ glass under 16 GPa pressure (broken lines).

for the intensity of the peak at 2.5 Å^{-1}, and show that an increase weighting factor for the Ge-Ge partial leads to an increased intensity for the 2.5 Å^{-1} peak with respect to neutron scattering.

E. Densified germania

Densification of the system has been performed by reproducing the usual experimental conditions, i.e., starting from a glass at ambient conditions (300 K and $\rho_g=3.66$ g cm^{-3}) and applying pressure up to 16 GPa. With pressure release from 15.2 GPa (the corresponding density is $\rho=5.9$ g cm^{-3}), the data of Price and co-workers [65] were qualitatively recovered; i.e., we obtained a final density $\rho=4.5$ g cm$^{-3}=1.25\rho_g$ in the decompressed system at zero pressure, as compared with $1.11\rho_g$ in the experimental sample.

The calculation of the pair correlation functions (not displayed) under pressure shows there are very weak changes in Ge-Ge and Ge-O bond distances in permanently densified system while the O-O distance decreases substantially (from 2.81 to 2.66 Å). Concerning the Ge-O distance, Itié *et al.* [8] have shown that this distance is the most sensitive one when going from the normal glass to the densified one as it increases drastically up to very high pressures (from 1.73 to 1.86 Å at 29.1 GPa). The present simulation shows a
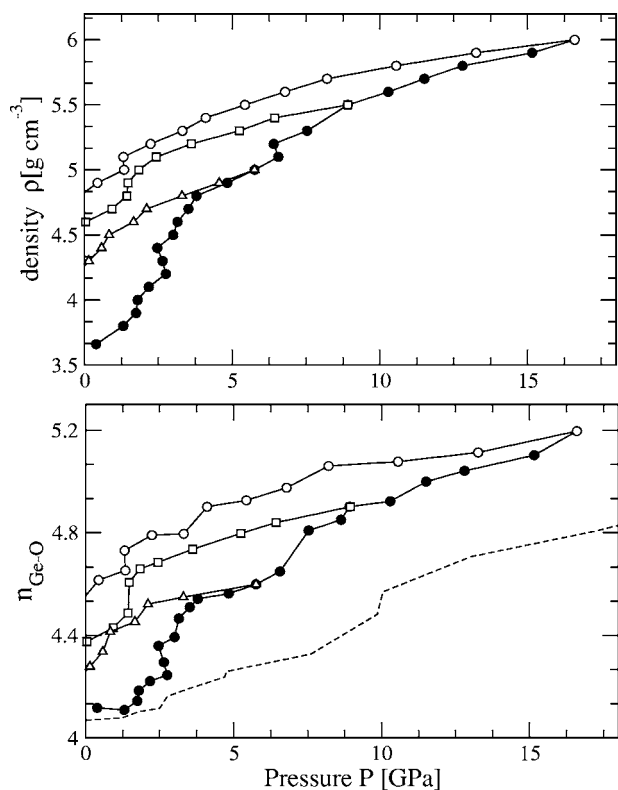
FIG. 11. Upper panel: Density change with applied pressure (filled circles) and decompression from 16.6 GPa (open circles), 8.9 GPa (open boxes) and 5.8 GPa (open triangles). Lower panel: Ge-O coordination number variation with pressure under compression and decompression. The broken line shows the corresponding compression behavior in amorphous silica using the Tsuneyucki potential [59].

more moderate increase from 1.73 to 1.79 Å for the same applied pressure of $\simeq 30$ GPa, but the value $d_{Ge-O} = 1.73$ Å remains constant up to the applied pressure of 8.9 GPa, in agreement with [9]. Concerning the coordination numbers, the number of oxygen neighbors (see Fig. 11) around an germanium atom is modified from 4.1 to 4.5 between the normal and the densified glass at $P \simeq 3$ GPa, which corresponds to a mean fraction x_6 of sixfold-coordinated germanium atoms of 0.05 and 0.27, respectively. With pressure, the number of oxygen neighbors in the vicinity of a germanium atom increases even more (Fig. 11) which suggests that pressure-induced densification is mostly achieved by the tetrahedral to octahedral conversion of the local structure. Thus, the change in local structure in the pressurized system at 16.6 GPa shows substantial differences in the bond distances ($d_{Ge-Ge} = 3.25$ Å, $d_{Ge-O} = 1.75$ Å and $d_{O-O} = 2.56$ Å) with respect to the glass at ordinary density ρ_g. Although it increases steadily with the pressure, the number of oxygen atoms around a Ge atom reaches slowly the octahedral limit [about $n_{Ge-O} = 5.2$ at 16.6 GPa; i.e., $x_6 = 0.85$ and 5.7 at 29.3 GPa ($x_6 = 0.85$)]. However, the coordination number increases much more rapidly in GeO_2 as in silica (broken line, Fig. 11). Finally, we note that the density change parallels the Ge-O bond distance change (Fig. 11).

Correspondingly, the FSDP in the neutron structure factor tends to disappear with pressure (see Fig. 12). This is due to
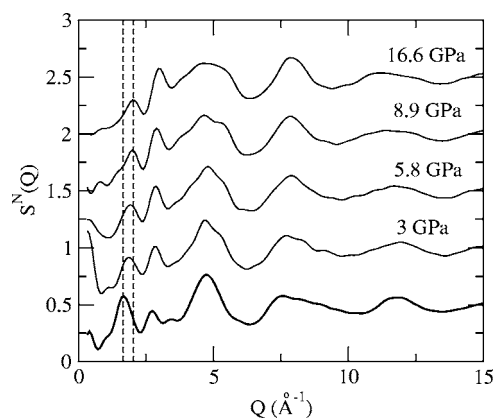

FIG. 12. Neutron structure factor evolution with applied pressure in amorphous GeO_2. The lower curve corresponds to the glass at zero pressure (density ρ_g). The vertical broken lines indicate the positions of the peaks of interest (see text for details).

the weakening of the first peak in the Ge-Ge partial structure factor which shifts from 1.65 to 2.49 Å^{-1}, leading to a global decrease of the long-range correlations. This general trend is similar to the one observed by Price and co-workers (specifically, see the difference structure factors in Ref. [65]).

IV. THE LIQUID STATE

A. Evolution of the structure with temperature

Starting from T_g, it is interesting to see how the structure is changed when the temperature is increased. The results correlate rather well with the findings of Kamiya *et al.* [38] who reported that at $T = 1425$ K, the Ge-Ge distances are shifted from 3.16 to 3.25 Å, an increase corroborated by Zarzycki [72], who found $d_{Ge-Ge} = 3.30$ Å at $T = 1475$ K. On the other hand, the Ge-O bond distance remains constant between the glassy state and the liquid at the aforementioned temperatures [38].

The present simulation shows that there is a slight shift in the Ge-O bond distance between the glassy and the liquid state (see Fig. 13) of about 0.03 Å, while the germanium-germanium distance remains mostly unchanged. The oxygen-oxygen bond distance changes from 2.81 to 2.85 Å and the corresponding peak in g_{OO} pair distribution function is lowered, leading to a broad peak centered at around 3.1 Å at $T = 1373$ K in the total neutron pair correlation function $T(r)$.

B. Thermodynamical portrait and equation of state

In order to evaluate the equation of state (EOS) of the liquid, we have computed a great number of thermodynamic points (T, ρ, P) and then analyzed the data using an analytical EOS. The data basis is made of 269 state points covering the following range: $0.5 \leq \rho \leq 5.5$ g cm^{-3} and $1500 \leq T \leq 5000$ K, the computed pressure being: $-1.13 \leq P \leq 33$ GPa. In contrast with previous work on molecular fluids [73,74] and silica, where a Van der Waals type EOS was used to obtain both the saturation line and the critical point, we adopt here a slightly different approach. We
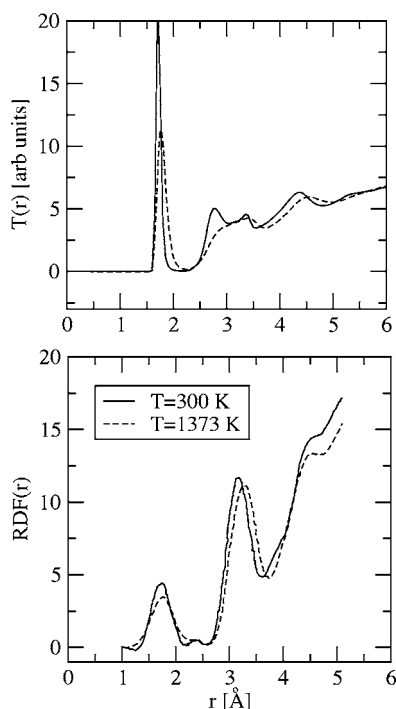
FIG. 13. Upper panel: Computed neutron pair correlation function $T(r)$ in the glass at 300 K (solid line, same as in Fig. 8) and in the melt at $T=1373$ K (broken line). Lower panel: experimental radial distribution function obtained from x-ray scattering [38] at the same temperatures.
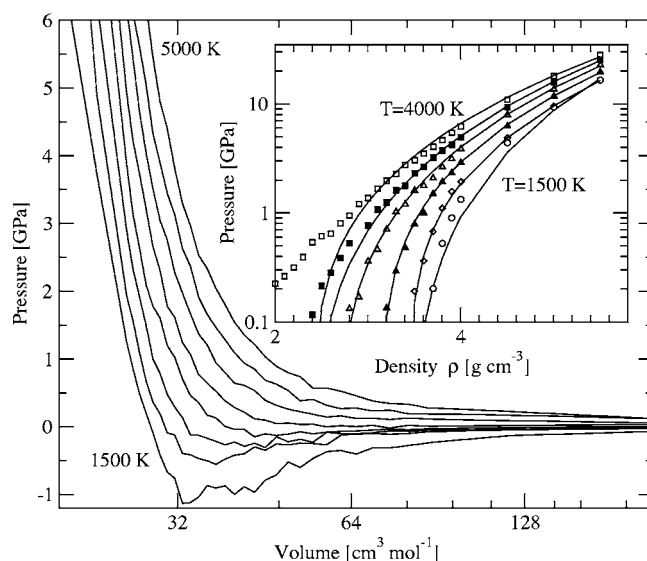

FIG. 14. Isotherms for liquid germania from the low-temperature to the critical region $(1500 \text{ K} \leq T \leq 5000 \text{ K})$. The curves are separated by 500 ± 40 K each. The inset shows the corresponding data in (ρ, P) together with the BM fits (solid lines).

fit the data with a Birch-Murnhagan equation of state BM EOS that has a simpler form [75,76]. It gives reasonable fits of solid and molten phases and is widely used in geophysical studies [77].

The isotherms of liquid germania in the (P, V) representation are displayed in Fig. 14. We have fitted the computed points far from the critical region with the BM EOS that has the following form:

$$P = \frac{3}{2}K\left(\left[\frac{\rho}{\rho_0}\right]^{7/3} - \left[\frac{\rho}{\rho_0}\right]^{5/3}\right)\left[1 - \frac{3}{4}[4 - K_1]\left(\left[\frac{\rho}{\rho_0}\right]^{2/3} - 1\right)\right], \tag{8}$$

where K is the bulk modulus, $K_1 = dK/dP$, and ρ_0 is the density, where the pressure of the liquid equals zero. Another advantage of using the BM EOS is that one has also access from Eq. (8) to the behavior of the isothermal compressibility $\kappa_T = \rho^{-1}(\partial \rho / \partial P)_T$ of the liquid with respect to the density (see Fig. 15). In germania, the latter quantity has been roughly evaluated [78] from a collection of experimental data. Specifically, Sekiya and co-workers [79] have measured densities in the liquid up to 1450 °C while expansivities have been measured [78] from the glass to the liquid at 1660 °C. Combining these data sets and other density data [80] along the isotherm 1425 °C, a polynomial [78] EOS was proposed by Dingwell et al. (out of which is calculated the compressibility κ_T, see broken line in Fig. 15). The latter appears to be clearly unrealistic as κ_T tends to saturate at low density. One should expect exactly the opposite behavior;

i.e., with falling density the compressibility should be enhanced. The present simulation permits first to compare our results with this estimate and also to calculate thermal quantities of the liquid for any other temperature. The fit can be realized with two parameters only (K and K_1) as ρ_0 corre-
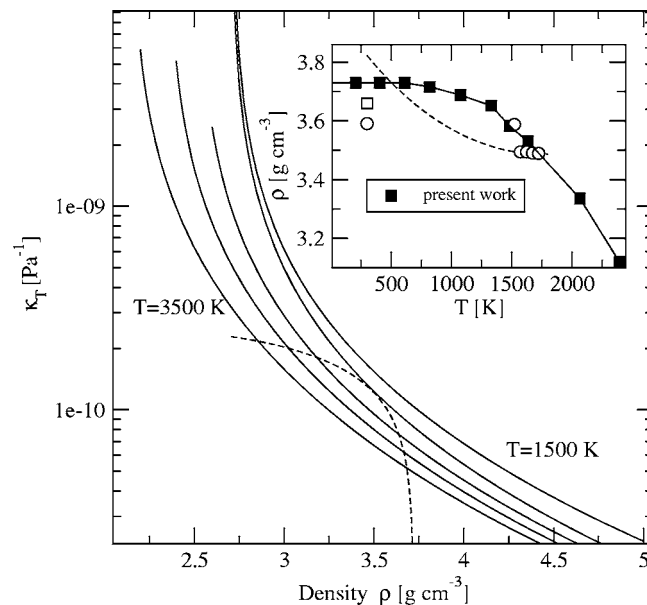

FIG. 15. Isothermal compressibility κ_T with respect to density in liquid GeO_2 for various temperatures ranging from 3500 to 1500 K separated by 500 K each (solid lines). The curves are computed using our BMEOS. The dashed line is extracted from a polynomial volume-pressure relationship obtained by Dingwell et al. [78] (see text for details) for $T \simeq 1700$ K. The inset shows along the liquid-vapor coexistence curve the computed density change with temperature (filled boxes), compared with experimental data from [38] (open box) and [78] (open circles). The broken line is a fit performed by Dingwell and co-workers [78].

sponds to the density of the liquid at zero pressure and can be accessed from the isothermal data displayed in Fig. 14. Several remarks can furthermore be made. (i) The zero-pressure density ρ_0 can be determined as long as the density of the system is large enough, i.e., larger than densities that are typical of the critical region [39]. ρ_0 falls from the value ρ_g at low temperature (1500 K) to 0.54 g cm^{-3} for 4000 K. For larger temperatures (i.e., $T \geq 4000$ K), there was need to fit the BMEOS with three parameters including ρ_0. (ii) The BMEOS can be considered as valid in the liquid phase for a large range of densities as long as the temperature is not too high. It deviates for densities smaller than $\simeq 2$ g cm^{-3} (inset of Fig. 14). The simulation provides an estimate of the compressibility that is very close to the one accessed from the experimentally studied densities. From Fig. 15, one can furthermore notice that the agreement (between polynomial fit and simulation) is best obtained in the vicinity of the glass density $\rho_g = 3.66$ g cm^{-3}. We find at $T = 2000$ K a value $\kappa_T = 9.13 \times 10^{-11}$ Pa^{-1}, while experimentally [78] it is found at $T \simeq 1700$ K, $\kappa_T = 12.4 \times 10^{-11}$ Pa^{-1}. Finally, the direct molecular dynamics method [45] permits us to predict the density change at zero pressure with temperature (inset of Fig. 15), which shows a rapid drop of ρ when the temperature is somewhat larger than 1300 K, in agreement with thermal expansion measurements [78].

V. SUMMARY AND CONCLUSIONS

We have discussed the results of a molecular dynamics simulation of germania glass and liquid by using the Oeffner-Elliott potential. This potential seems rather reliable as it permits us to reproduce reasonably well the structural properties of the system. The enthalpy change during the glass transition and the glass transition temperature itself appear to be very close to the experimental data. However, during the investigation, several limitations of this potential have appeared, such as the severe overestimation of the self-diffusion constants, although consistent with previous findings for silica, which poses the problem of the accurate simulation of the dynamics of strong glass-forming liquid. Thermodynamical quantities of the liquid such as pressure and compressibility have been computed within this model and provide via the Birch-Murnhagan equation of state new estimates that gain some accuracy with respect to previous analytical evaluations.

Some of the quantities calculated in the present paper lie in a temperature and pressure range that are now accessible by experiment. The realization of calorimetric or dilatometric measurements would permit one to check that the Oeffner-Elliott potential is not only reliable for the ordinary and densified glass but also in the liquid state.

[1] L. Liu, W. A. Bassett, and J. Sharry, J. Geophys. Res. **83**, 2301 (1978).

[2] L. C. Ming and M. H. Manghnani, Phys. Earth Planet. Inter. **33**, 26 (1983).

[3] S. R. Elliott, *Physics of Amorphous Materials* (Wiley, New York, 1989).

[4] A. C. Wright, G. Etherington, J. A. Erwin Desa, R. N. Sinclair, G. A. N. Connel, and J. C. Mikkelson, J. Non-Cryst. Solids **49**, 63 (1982); L. G. Van Uitert, J. Appl. Phys. **50**, 8052 (1979).

[5] J. H. Konnert, J. Karle, and G. A. Ferguson, Science **179**, 177 (1973).

[6] J. Hertling, S. Baessler, S. Rau, G. Kasper, and S. Hunklinger, J. Non-Cryst. Solids **226**, 129 (1998).

[7] F. S. El'kin, V. V. Brazhkin, L. G. Khvostantsev, O. B. Tsiok, and A. G. Lyapin, JETP Lett. **75**, 342 (2002); O. Ohtaka, H. Arima, H. Fukui, W. Utsumi, Y. Katayama, and A. Yoshiasa, Phys. Rev. Lett. **92**, 155506 (2004).

[8] J. P. Itié, A. Polian, G. Calas, J. Petiau, A. Fontaine, and H. Tolentino, Phys. Rev. Lett. **63**, 398 (1989).

[9] C. Meade, R. J. Hemley, and H. K. Mao, Phys. Rev. Lett. **69**, 1387 (1992).

[10] S. Sugai and A. Onodera, Phys. Rev. Lett. **77**, 4210 (1996).

[11] P. Richet, G. Hovis, and B. Poe, Chem. Geol. **213**, 41 (2004).

[12] D. J. Lacks, Phys. Rev. Lett. **84**, 4629 (2000).

[13] For a recent review, see: C. A. Angell, Annu. Rev. Phys. Chem. **55**, 559 (2004).

[14] J. L. Finney, D. T. Bowron, A. K. Soper, T. Loerting, E. Mayer, and A. Hallbrucker, Phys. Rev. Lett. **89**, 205503 (2002).

[15] I. Okabe, H. Tanaka, and K. Nakanishi, Phys. Rev. E **53**, 2638 (1996); P. H. Poole, F. Sciortino, U. Essmann, and H. E. Stanley, Nature (London) **360**, 324 (1992); Phys. Rev. E **48**, 3799 (1993).

[16] M. Durandurdu and D. A. Drabold, Phys. Rev. B **66**, 041201 (2002).

[17] E. G. Ponyatovskii and O. I. Barkalov, Mater. Sci. Rep. **8**, 147 (1992).

[18] K. O. Trachenko, M. T. Dove, M. J. Harris, and V. Heine, J. Phys.: Condens. Matter **12**, 8041 (2000).

[19] K. Kamiya, T. Yoko, Y. Miki, Y. Itoh, and S. Sakka, J. Non-Cryst. Solids **91**, 279 (1987).

[20] D. L. Price, A. J. G. Ellison, M. L. Saboungi, R. Z. Hu, T. Egami, and W. S. Howells, Phys. Rev. B **55**, 11249 (1997).

[21] T. Furukawa and W. B. White, J. Mater. Res. **15**, 1648 (1980).

[22] C. Yin, K. Lu, and Y. Zhao, J. Non-Cryst. Solids **112**, 96 (1989).

[23] G. S. Henderson and M. E. Fleet, J. Non-Cryst. Solids **134**, 259 (1991).

[24] F. L. Galeener, A. J. Leadbetter, and M. W. Stringfellow, Phys. Rev. B **27**, 1052 (1983).

[25] D. J. Durben and G. H. Wolf, Phys. Rev. B **43**, 2355 (1991).

[26] G. Gutierrez and J. Rogan, Phys. Rev. E **69**, 031201 (2004).

[27] P. Vashishta, R. K. Kalia, J. P. Rino, and I. Ebbsjö, Phys. Rev. B **41**, 12197 (1990).

[28] J. Sarnthein, A. Pasquarello, and R. Car, Phys. Rev. Lett. **74**, 4682 (1995); Phys. Rev. B **52**, 12690 (1995).

[29] L. V. Woodcock, C. A. Angell, and P. Cheeseman, J. Chem. Phys. **65**, 1565 (1976).

[30] P. F. McMillan, in *Structure, Dyamics and Properties of Silicate Melts*, edited by J. Stebbins, P. F. McMillan, and D. Dingwell, in Rev. Mineralogy Vol. 32 (Miner. Soc. America, Washington, D.C., 1995).

[31] R. D. Oeffner and S. R. Elliott, Phys. Rev. B **58**, 14791 (1998).

[32] D. M. Christie and J. R. Chelikowsky, Phys. Rev. B **62**, 14703 (2000).

[33] T. Tsuchiya, T. Yamanaka, and M. Matsui, Phys. Chem. Miner. **25**, 94 (1998).

[34] Z. Lodziana, K. Parlinski, and J. Hafner, Phys. Rev. B **63**, 134106 (2001).

[35] T. Tsuchiya, T. Yamanaka, and M. Matsui, Phys. Chem. Miner. **27**, 149 (2000).

[36] J. R. Rustad, D. A. Yuen, and F. J. Spera, Phys. Rev. A **42**, 2081 (1990).

[37] A. B. Belonoshko, Geochim. Cosmochim. Acta **58**, 1557 (1994).

[38] K. Kamiya, T. Yoko, Y. Itoh, and S. Sakka, J. Non-Cryst. Solids **86**, 385 (1985).

[39] B. Guillot and Y. Guissani, J. Chem. Phys. **104**, 7633 (1996).

[40] K. Vollmayr, W. Kob, and K. Binder, Phys. Rev. B **54**, 15808 (1996).

[41] X. Feng, W. J. Bresser, and P. Boolchand, Phys. Rev. Lett. **78**, 4422 (1997).

[42] D. Caprion and H. R. Schober, Phys. Rev. B **62**, 3709 (2000).

[43] H. He and M. F. Thorpe, Phys. Rev. Lett. **54**, 2107 (1985).

[44] K. Trachenko and M. T. Dove, Phys. Rev. B **67**, 064107 (2003).

[45] J. Alejandre, D. Tildesley, and G. A. Chapela, J. Chem. Phys. **102**, 4574 (1995).

[46] P. Richet, Phys. Chem. Miner. **17**, 79 (1990).

[47] P. Richet and Y. Bottinga, Rev. Geophys. **24**, 1 (1986).

[48] C. A. Angell and J. C. Tucker, *Physical Chemistry of Process Metallurgy*, in The Richardson Conference (Inst. Mining Metall Publ., London, 1974), pp. 207.

[49] D. G. Georgiev, P. Boolchand, and M. Micoulaut, Phys. Rev. B **62**, R9228 (2000).

[50] P. Boolchand (private communication).

[51] J. Horbach and W. Kob, Phys. Rev. B **60**, 3169 (1999).

[52] T. Tokuda and W. D. Kingery, J. Appl. Phys. **34**, 2104 (1963).

[53] See, e.g., A. Sipp, Y. Bottinga, and P. Richet, J. Non-Cryst. Solids **288**, 166 (2001).

[54] S. Glasstone, K. J. Laider, and H. Eyring, *The Theory of Rate Processes* (McGraw-Hill, New York, 1941).

[55] B. O. Mysen and P. Richet, *Silicate Glasses and Melts: Structure and Properties* (Springer, Berlin, 2005).

[56] G. Brebec, R. Seguin, C. Sella, J. Benevot, and J. C. Martin, Acta Metall. **28**, 327 (1980).

[57] J. C. Mikkelsen, Appl. Phys. Lett. **45**, 1187 (1984).

[58] In using the Tsuneyuki (TTAM, [59]) potential, Della Valle and Venuti [60], and Guissani and Guillot [39], both found a T_g around 2000 K, much lower than for the BKS potential using similar computational parameters. In fact, the TTAM model was simulated at the experimental density 2.2 g/cm^3, while the BKS potential was run at a density higher corresponding to zero pressure, leading to an increase of the diffusion coefficients and an increase of the apparent T_g with respect to the TTAM T_g.

[59] S. Tsuneyuki, M. Tsukada, H. Aoki, and Y. Matsui, Phys. Rev. Lett. **61**, 869 (1988).

[60] R. G. Della Valle and E. Venuti, Chem. Phys. **179**, 411 (1994).

[61] D. L. Price, M. L. Saboungi, and A. C. Barnes, Phys. Rev. Lett. **81**, 3207 (1998).

[62] R. Hussin, R. Dupree, and D. Holland, J. Non-Cryst. Solids **246**, 159 (1999).

[63] C. E. Stone, A. C. Hannon, T. Ishihara, N. Kitamura, Y. Shirakawa, R. N. Sinclair, N. Umesaki, and A. C. Wright, J. Non-Cryst. Solids **293–295**, 769 (2001).

[64] L. Koester, H. Rauch, M. Herkens, and K. Schröder, Jülich Report, Jül-1755, 1981.

[65] S. Sampath, C. J. Benmore, K. M. Lantzky, J. Neuefeind, K. Leinenweber, D. L. Price, and J. L. Yarger, Phys. Rev. Lett. **90**, 115502 (2003).

[66] Y. Waseda, K. Sugiyama, E. Matsubara, and K. Harada, Mater. Trans., JIM **31**, 421 (1990).

[67] P. Vashishta, R. K. Kalia, J. P. Rino, and I. Ebbsjö, Phys. Rev. B **41**, 12197 (1990).

[68] C. Massobrio, A. Pasquarello, and R. Car, Phys. Rev. Lett. **80**, 2342 (1998).

[69] D. L. Price, S. C. Moss, R. Reijers, M. L. Saboungi, and S. Susman, J. Phys.: Condens. Matter **1**, 1005 (1989).

[70] D. L. Price, A. J. G. Ellison, M. L. Saboungi, R. Z. Hu, T. Egami, and W. S. Howells, Phys. Rev. B **55**, 11249 (1997).

[71] Specifically, see Fig. 3 in S. Kohara and K. Suzuya, J. Phys.: Condens. Matter **17**, S77 (2005).

[72] J. Zarzycki, Verres Refract. **11**, 3 (1957).

[73] F. H. Ree, J. Chem. Phys. **73**, 5401 (1980).

[74] B. Guillot and Y. Guissani, J. Chem. Phys. **98**, 8221 (1993).

[75] F. Birch, J. Geophys. Res. **57**, 227 (1951).

[76] S. K. Saxena, N. Chatterjee, Y. Fei, and G. Shen, *Thermodynamic Data on Oxydes and Silicates* (Springer, New York, 1993).

[77] See, e.g., C. B. Agee, Phys. Earth Planet. Inter. **107**, 63 (1998).

[78] D. B. Dingwell, R. Knoche, and S. L. Webb, Phys. Chem. Miner. **19**, 445 (1993).

[79] K. Sekiya, K. Morinaga, and T. Yanagase, J. Ceram. Soc. Jpn. **88**, 367 (1980).

[80] C. M. Scarfe, B. O. Mysen, and D. Virgo, Geochem. Soc. Spec. Publ. **1**, 59 (1987).